AGU PUBLICATIONS

JGR

Journal of Geophysical Research: Oceans

RESEARCH ARTICLE

10.1002/2017JC012999

Brine Convection, Temperature Fluctuations, and Permeability in Winter Antarctic Land-Fast Sea Ice

P. Wongpan[1], K. G. Hughes[1,2], P. J. Langhorne[1], and I. J. Smith[1]

[1]Department of Physics, University of Otago, Dunedin, New Zealand, [2]School of Earth and Ocean Sciences, University of Victoria, Victoria, British Columbia, Canada

Abstract Vertical temperature strings are used in sea ice research to study heat flow, ice growth rate, and ocean-ice-atmosphere interaction. We demonstrate the feasibility of using temperature fluctuations as a proxy for fluid movement, a key process for supplying nutrients to Antarctic sea ice algal communities. Four strings were deployed in growing, land-fast sea ice in McMurdo Sound, Antarctica. By smoothing temperature data with the robust LOESS method, we obtain temperature fluctuations that cannot be explained by insolation or atmospheric heat loss. Statistical distributions of these temperature fluctuations are investigated with sensitivities to the distance from the ice-ocean interface, average ice temperature, and sea ice structure. Fluctuations are greatest close to the base (<50 mm) at temperatures >-3°C, and are discrete events with an average active period of 43% compared to 11% when the ice is colder (–3°C to -5°C). Assuming fluctuations occur when the Rayleigh number, derived from mushy layer theory, exceeds a critical value of 10 we approximate the harmonic mean permeability of this thick (>1 m) sea ice in terms of distance from the ice-ocean interface. Near the base, we obtain values in the same range as those measured by others in Arctic spring and summer. The permeability between the ice-ocean interface and 0.05 ± 0.04 m above it is of order 10^{-9} m^2. Columnar and incorporated platelet ice permeability distributions in the bottom 0.1 m of winter Antarctic sea ice are statistically significantly different although their arithmetic means are indistinguishable.

Key Points:
- Observed temperature fluctuations of ~0.01°C and shorter than 12 h are proxies for brine convection in sea ice
- Temperature fluctuations in thick, growing, Antarctic sea ice occur sporadically near the ice-ocean interface where temperature is >−3°C
- Near the ice-ocean interface, in situ estimates of columnar and incorporated platelet ice permeability overlap, and agree with previous work

Correspondence to:
P. Wongpan,
pat.wongpan@postgrad.otago.ac.nz

Citation:
Wongpan, P., Hughes, K. G., Langhorne, P. J., & Smith, I. J. (2018). Brine convection, temperature fluctuations, and permeability in winter Antarctic land-fast sea ice. *Journal of Geophysical Research: Oceans*, *123*, 216–230. https://doi.org/10.1002/2017JC012999

Received 17 APR 2017
Accepted 14 DEC 2017
Accepted article online 27 DEC 2017
Published online 12 JAN 2018

1. Introduction

The interface between sea ice and the ocean is a dynamic and biologically active layer (Tedesco et al., 2010), where fluid transport facilitates the resupply of nutrients to Antarctic land-fast sea ice algal communities (Reeburgh, 1984; Vancoppenolle et al., 2010). A key mechanism for fluid transport is gravity drainage or brine convection (Cox & Weeks, 1975; Notz & Worster, 2009; Worster & Rees Jones, 2015; Untersteiner, 1968), a process that can be expressed in the mushy-layer framework (Feltham et al., 2006). In its simplest form a mushy layer is a two-phase (solid and liquid), two-component (for sea ice, pure ice, and brine), reactive porous medium for which the flow alters the structure of the material (Feltham et al., 2006; Worster & Rees Jones, 2015). Convection begins when a local Rayleigh number exceeds a critical value (Wettlaufer et al., 1997a; Worster, 1992; Worster & Rees Jones, 2015) with the desalination rate a function of the Rayleigh number (Rees Jones & Worster, 2014; Worster & Rees Jones, 2015). With the ability to produce dynamic salinity profiles (Griewank & Notz, 2013; Rees Jones & Worster, 2014; Turner et al., 2013), mushy layer desalination has been implemented in the widely used sea ice thermodynamic model CICE (Turner & Hunke, 2015).

During sea ice growth, as illustrated in Figure 1b, cold, salty, and dense brine is drained by gravity through brine channels which are distributed to maximize brine rejection (Wells et al., 2010, 2011). That brine is then replaced by fresher, warmer, and less dense sea water from the ocean through the porous sea ice (Lake & Lewis, 1970; Niedrauer & Martin, 1979; Weeks, 2010; Worster & Rees Jones, 2015). In natural sea ice Pringle et al. (2007) recorded thermal signatures attributed to brine convection events with time scales of several hours. These occurred 22 times over 1,957 days (Pringle et al., 2007), confirming that episodic convection associated with desalination takes place in the region close to the ice-ocean interface (Lake & Lewis, 1970). In smaller scale laboratory experiments, Eide and Martin (1975) described flow oscillations within brine tubes with upflows lasting 8–15 min and outflows lasting 45 min. Further, the coldest temperatures were recorded by the sensor closest to the brine channel (Niedrauer & Martin, 1979) where records showed a convective temperature signal-to-noise ratio of 100, with 0.01°C (10 mK) noise amplitude. Alternatively,

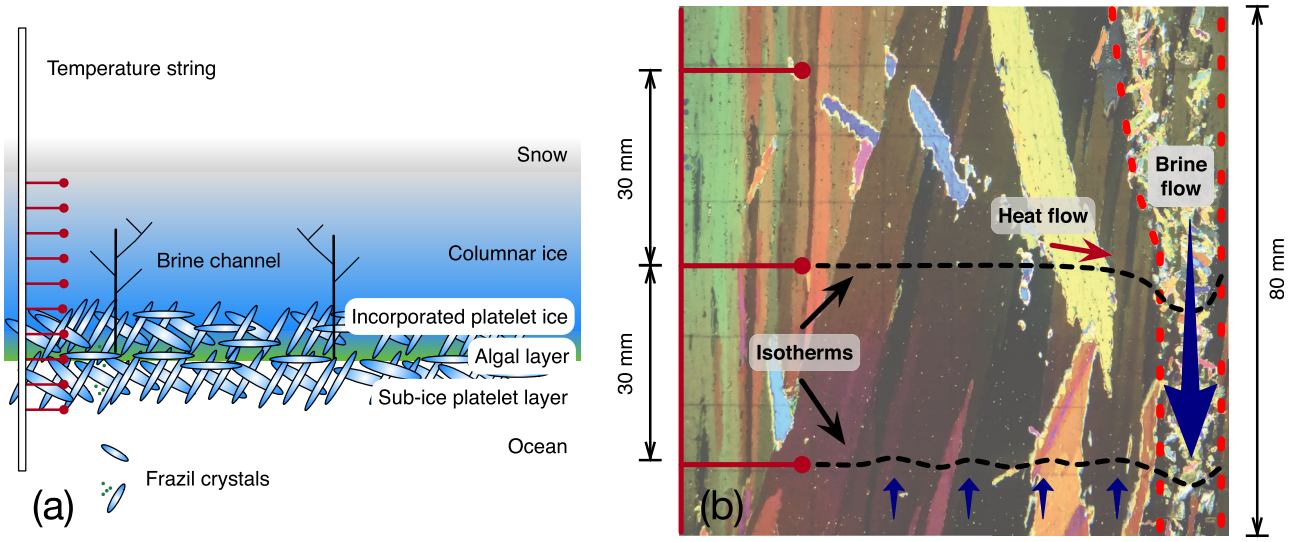

Figure 1. (a) Schematic diagram of the temperature string, sea ice structures, brine channel, and algal layer. (b) Brine drainage and compensating upward flow overlaid on a vertical thin section of incorporated platelet ice. The brine drainage channel (outlined by red dashed lines) is refrozen because of the low thin section temperature ($\approx -20^{\circ}$C). Thermistors are illustrated with red pins on the left. Cold and dense brine moves downward and is replaced by warmer and less dense brine from below indicated with big and small blue arrows, respectively. This movement perturbs the isotherms (black dashed lines). Heat then flows (red arrows) to re-equilibrate the isotherms which can be captured by the thermistors as temperature fluctuations. Note that between the brine channel and the thermistor there could be other heat sources/sinks due to exchanging brine with the water column through the porous sea ice. This interpretation follows Lake and Lewis (1970), Maksym and Jeffries (2000), and Worster and Rees Jones (2015).

optical methods allow a better visualization of convective processes, albeit under particularly artificial conditions. From a 4 h observation of brine flow, Middleton et al. (2016) noted that brine channels were active for an average of 81% of the time.

Predicting and quantifying brine convection in situ is challenging: permeability, arguably the most relevant parameter, varies spatially and temporally (Worster, 1992) and in sea ice it is dependent on ice porosity (Eicken et al., 2004; Freitag, 1999; Freitag & Eicken, 2003; Petrich et al., 2006; Polashenski et al., 2017). The reported values of permeability in sea ice vary by orders of magnitude. For example, Freitag and Eicken (2003) and Polashenski et al. (2017) made measurements of permeability using in situ bail tests in Arctic spring or summer sea ice and reported vertical permeabilities in the range of 10^{-13} to 10^{-7} m^2. In sea ice vertical permeability is typically 10 times greater than horizontal permeability (Freitag & Eicken, 2003; Petrich et al., 2006). Measurements of sea ice permeability in the literature are sparse (Petrich et al., 2006, and references therein), but Freitag (1999) and Eicken et al. (2004) provide formulae to compute the vertical permeability of columnar sea ice from its porosity. Rees Jones and Worster (2014) reanalyzed laboratory data of Wettlaufer et al. (1997a) to obtain a bulk permeability by using a local Rayleigh number to determine the thickness of the convecting layer.

Here we use a similar method, but instead monitor the temperature at a prescribed depth and presume that the local Rayleigh number, based on the harmonic mean permeability of the layer beneath, has exceeded the critical Rayleigh number if temperature fluctuations are observed. Using this technique we examine the permeability of columnar and incorporated platelet ice, the latter ubiquitous in our study site of McMurdo Sound (Langhorne et al., 2015). Gough et al. (2012a) report that the bulk salinity of incorporated platelet ice and columnar ice are very similar, so a comparison of permeability between these ice structures may help explain this observation. Although platelet ice is a habitat that hosts the highest concentration of sea ice algae on Earth (Arrigo et al., 2010), its permeability has not been estimated before.

In this paper, we define the spatial and temporal statistics of temperature fluctuations associated with brine movement in thick, winter, land-fast sea ice (section 2.2). We note how these statistics depend upon mean ice temperature (section 3.1), and provide in situ experimental evidence in natural sea ice that there is confinement of convection in a layer at the base of the sea ice (section 3.2), probably due to strongly varying permeability (Notz & Worster, 2008). Combining temperature string data with sea ice structure analysis

provides us with a framework to study temperature fluctuations across a structural transition from columnar to incorporated platelet ice, which has never been reported before. Finally, we estimate the permeability of growing, Antarctic land-fast sea ice over a time period of more than four months for three separate winters (section 3.4).

2. Data and Methods

2.1. Temperature Data

The vertical temperature strings used in this paper have been designed to measure heat flow through sea ice, sea ice growth rate, and thermal properties (e.g., Gough et al., 2012b; Pringle et al., 2007; Smith et al., 2012; Trodahl et al., 2000). Temperature variations near the air-ice interface primarily respond to meteorological forcing (such as insolation) and snow cover, whereas variations near the ice-ocean interface reflect oceanographic conditions. Sea ice acts as a low-pass filter for temperature signals propagating from the air-ice interface, i.e., the air temperature signal is smoothed and damped with increasing depth into the ice. Following Lewis (1967), we find that for the data discussed in this paper, on average, it took 60 h for a temperature variation at the ice-snow interface to propagate through 1 m thick sea ice. Therefore, in the same manner as Lake and Lewis (1970), we argue that shorter time scale temperature changes at the base of thick sea ice require fluid motion. To study the phenomena arising from the exchange of brine at the base, we focus on temperature variations with periods of less than 24 h.

The temperature strings were installed through growing first-year, land-fast sea ice in McMurdo Sound, Antarctica (Figure 2). We use four temperature string data sets from three different years: 2009, 2010, and 2013 (Table 1). Strings used in 2009 are described by Gough et al. (2012a, 2012b). Those used in 2010 and 2013, which have variable spatial resolution with depth, share the same string design described by Trodahl et al. (2000). All thermistors have a noise floor of 10^{-3}°C or better.

At the locations of our sites (Figure 2), in situ supercooling is frequently observed close to the ocean surface during winter (e.g., Leonard et al., 2011) and platelet ice is a feature of the sea ice cover (e.g., Gough et al., 2012b; Smith et al., 2012). The ice thickness at which incorporated platelet ice first forms was measured from cores extracted close to the strings at the end of each observation period. This is termed the incorporated platelet ice transition in Table 1. 2009A and the top part of 2009B (2009B CI) were deployed in columnar ice, while the bottom part of 2009B (2009B PI), 2010, and 2013 monitored incorporated platelet ice.

The full time series from 2009B is shown in Figure 3. Data were calibrated by being brought to a constant value in the ocean (Gough et al., 2012b). As illustrated in Figure 3c, after the freezing front reached a

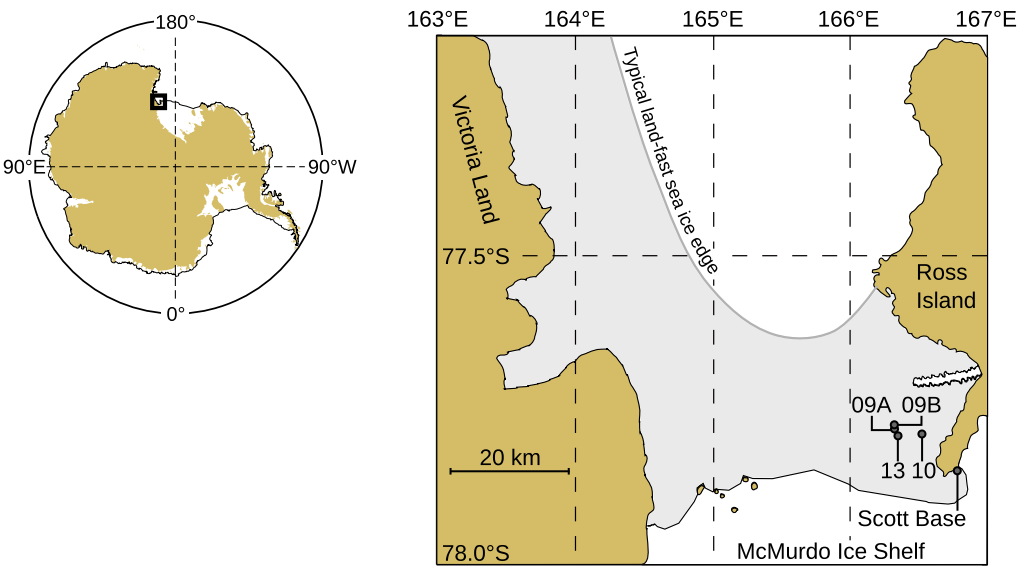

Figure 2. Thermistor strings were installed in eastern McMurdo Sound in 2009, 2010, and 2013. These sites are close to the McMurdo Ice Shelf and Scott Base, New Zealand's Antarctic logistics support base.

Table 1
Summary of Data Set Analyzed in This Paper

Study sites	Study period	Number of operating thermistors	Sampling intervals (min)	Incorporated platelet ice transition (m)	Deepest thermistor (m)	Spacing[a] (mm)	Resolution (°C)
2009A	May 5–Jul 16	11	4	1.50	1.4	30	2×10^{-3}
2009B	May 29–Nov 19	47	10	1.57	2.0	30	7×10^{-4}
2010	Jun 29–Nov 27	19	10	1.25	1.9	400, 100, 50	3×10^{-5}
2013	Jul 16–Nov 10	20	10	1.11	1.9	400, 100, 50	3×10^{-5}

[a]Note that the 2010 and 2013 temperature strings have variable spatial resolution with thermistors at depths 0.10, 0.50, 0.90, 1.00, 1.10, 1.20, 1.25, 1.30, 1.35, 1.40 (only for 2013), 1.45, 1.50, 1.55, 1.60, 1.65, 1.70, 1.75, 1.80, 1.85, and 1.90 m from the ice-air interface.

particular thermistor, that thermistor record quickly diverges from the records of thermistors that remain in the water (e.g., Gough et al., 2012b; Niedrauer & Martin, 1979). The times at which this occurred were estimated by inspection of the changing of slope in temperature, as described in Smith et al. (2012). Ice thickness as a function of time can then be determined by interpolating the resulting time and thermistor depth pairs. This allows calculation of the distance of any thermistor from the ice-ocean interface at any time.

2.2. Defining Temperature Fluctuations

Close to the ice-ocean interface, temperature fluctuations up to ~0.1°C can be observed (Figure 3d). Their signal-to-noise ratio is of order 100, making them easily resolvable. In order to detect whether the temperature fluctuations move upward or downward we have attempted to measure the lag between the events on adjacent thermistors. Unfortunately the sampling interval of our measurements is too great (4–10 min) for us to resolve this movement, and the fluctuation events appear "instantaneous" on adjacent thermistors. At each data point, we can extract a temperature fluctuation by subtracting the raw temperature from an appropriately defined background temperature, found here using the robust LOESS method (Cleveland, 1979).

Without reference to any physical variables other than time, the problem we set out to solve is to choose an appropriate method to smooth a signal under the following conditions: (i) any variation that appears to have a time scale of a day or longer should be fully captured in the smoothed curve and (ii) outlying data should have little-to-no influence on the smoothed curve. Note that we set no conditions for the distribution of residuals. For example, we are not concerned if the residual data contain many more troughs than peaks or vice versa.

To smooth our raw data, keeping the first condition in mind, we start with a method known as standard LOESS smoothing (Cleveland, 1979). In this method, the smooth curve at any time t is found by fitting a second-degree polynomial to the data contained in the window $t-\tau < t < t+\tau$, where τ is the half window width. In Figure 4b, following Cleveland (1979), the data points t_i within this window are weighted by their distance from t as described by the tricube function w_i

$$w_i = \left(1-\left|\frac{t-t_i}{2\tau}\right|^3\right)^3. \quad (1)$$

The only parameter that we need to specify is the window width, which we take to be 12 h, i.e., $\tau = 6$ h. By using a 12 h window, the smoothing can adequately capture any sinusoidal variation with a 24 h period. This satisfies our first condition.

There remains a problem with the standard LOESS method for our purposes: outliers influence the fitting of the polynomial and therefore the smoothed output. To overcome this problem, we use the robust LOESS method described by Cleveland (1979), which we implement with the smooth function in the MATLAB Curve Fitting Toolbox (version 3.5.3). With this method, the smoothed curve is fitted iteratively. Residuals are calculated after the first fit using the LOESS method. Outliers are given reduced weight in the subsequent fit. This iteration is undertaken five times in total. Figures 4a and 4b demonstrate how data outliers are ultimately given smaller or no weight to the fitted curve which fulfills our second condition.

From careful inspection, certain parts of our data sets are not well handled by our current smoothing procedure, such as rapidly growing ice, ice close to the ice-snow surface, or data within a window width at the

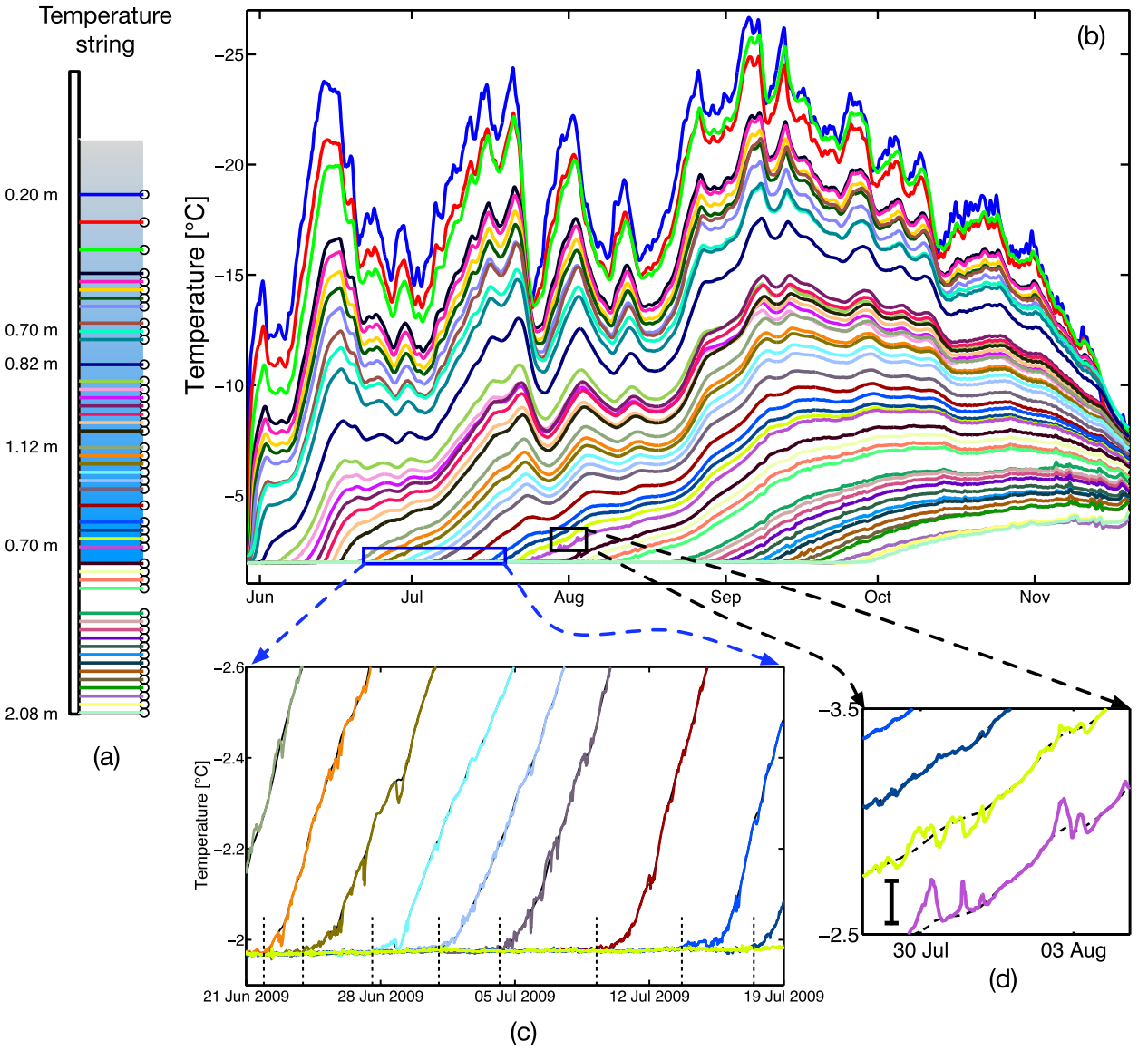

Figure 3. (a) Schematic diagram of a temperature string. (b) An example of a winter temperature string record (2009B). The entire string becomes frozen in by late September. The color of each thermistor sensor in Figure 3a corresponds to each trace of the temperature data in Figure 3b. Note that the temperature axis is inverted so that the top thermistor corresponds with the uppermost temperature trace. Regions of the data are enlarged in the plots to better show (c) an example of the consecutive freezing in of thermistors, and (d) a black vertical bar that indicates what we called a fluctuation (T') in this paper. Note that malfunctioning thermistors were removed from the analysis causing uneven spacings of the temperature string in Figure 3a.

start or end of the temperature variation. Hence, we will analyze only data that pass the following criteria: (i) they were recorded at least 5 days after the thermistor records began and (ii) they were recorded by thermistors deeper than 0.5 m. Note that robust LOESS smoothing is less successful at the edges of a curve as it cannot use a symmetrical weight function for any points within one span of the edges. Imposing the aforementioned conditions means we can ignore any smoothing artifacts that the edges introduce. These conditions are applied throughout this paper.

We are now in the position to extract temperature fluctuations (T') of timescales less than 12 h from our data sets by subtracting the smoothed background temperatures (T_{LOESS}) from the actual temperatures (T) using the robust LOESS method:

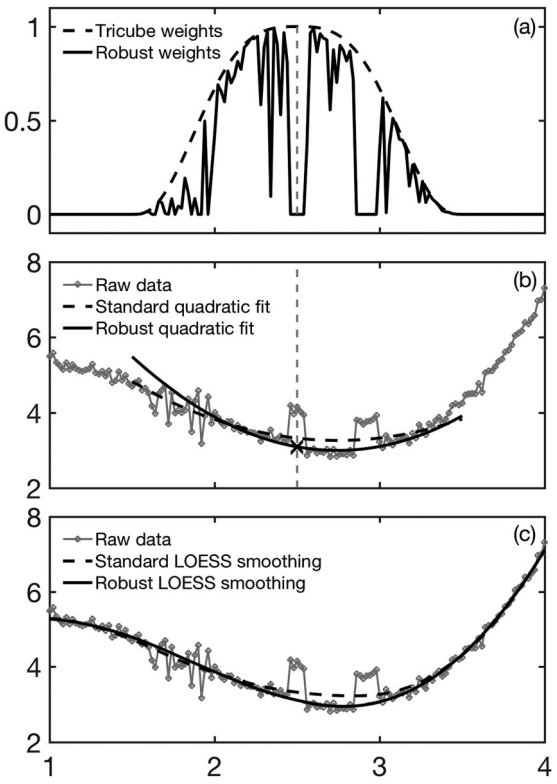

Figure 4. Example of standard and robust LOESS smoothing of arbitrary input data. The smoothing span is 2 units. (a) The weights (equation (1)) applied to each point in the fitting of the polynomial as determined by the tricube and robust functions centered on the point of interest, which is $t = 2.5$ in this example marked with vertical-dashed line. With the robust method, weights also depend on the size of the residual relative to the smoothed curve. (b) To find the smoothed output for $t = 2.5$, a second order polynomial is fit to all data in the region $1.5 < t < 3.5$ using the weights shown in Figure 4a. The smoothed output at $t = 2.5$ using the robust method is shown by the black cross. (c) The overall result after the process in Figures 4a and 4b has been repeated for every point.

$$T'(z,t) = T(z,t) - T_{\mathrm{LOESS}}(z,t), \tag{2}$$

where z is the distance from the air-ice interface and t is time. In section 3, we consider how T' varies statistically as a function of temperature and distance from the ice-ocean interface.

2.3. Estimation of Permeability From Temperature Fluctuations

We have argued that temperature fluctuations are proxies of fluid convection (Lake & Lewis, 1970; Niedrauer & Martin, 1979) and that the onset of convection starts when the Rayleigh number exceeds a critical value (Wettlaufer et al., 1997a; Worster, 1992; Worster & Rees Jones, 2015). The depth-dependent local Rayleigh number, which governs the onset and strength of convection in sea ice (e.g., Notz & Worster, 2008; Worster & Rees Jones, 2015), can be expressed as

$$R_m(z) = \frac{g\rho_\ell \beta \Delta S_b (h-z)\Pi_l(z)}{\kappa_{\mathrm{si}}\mu}, \tag{3}$$

where R_m is the local Rayleigh number at level z measured from the upper ice surface, ρ_ℓ is the density of ocean, and β is saline contraction coefficient. ΔS_b is the difference between the salinity of the ocean and the salinity at depth z. Assuming local thermodynamic equilibrium (Feltham et al., 2006), these are estimated from raw thermistor measurements in the respective locations using equation (3.4) of Notz (2005). h is the sea ice thickness, and $\Pi_l(z)$ is the local permeability. The distance from the interface is $d = h - z$, μ is viscosity and κ_{si} is the thermal diffusivity of the sea ice. Equation (3) can be rearranged to approximate the harmonic mean (or bulk) permeability Π, corresponding to the greatest distance from the ice-water interface (greatest d) at which fluid motion is detected

$$\Pi(z) \approx \frac{R_c \kappa_{\mathrm{si}}\mu}{g}\frac{1}{\rho_\ell \beta \Delta S_b d}, \tag{4}$$

where (Rees Jones & Worster, 2014),

$$\Pi(z) = \left[\frac{1}{h-z}\int_z^h \frac{1}{\Pi_l(z')}\,\mathrm{d}z'\right]^{-1}. \tag{5}$$

We argue that the critical Rayleigh number for the mushy layer is $R_c \approx 10$ (Worster, 1992; Worster & Rees Jones, 2015). Griewank and Notz (2013) used a robust parameter estimation approach to arrive at an R_c of about 1 by using the minimum permeability between the layer in question and the ice-ocean interface, but they later changed the value to roughly 5 after switching to a harmonic mean permeability (Griewank & Notz, 2015). Rees Jones and Worster (2014) also used the harmonic mean permeability with R_c of either 5, 20, or 40 as tuning parameters, and have demonstrated that a constant critical bulk Rayleigh number is consistent with a bulk permeability that varies cubically with mean porosity as suggested by Freitag (1999). Since we calculate R_m in equation (3) using the thermal diffusivity of sea ice (Notz & Worster, 2008; Wells et al., 2010, 2011; Worster & Rees Jones, 2015) rather than brine (as used by Griewank and Notz (2013) and Rees Jones and Worster (2014)), a critical Rayleigh number of approximately 10 is appropriate (Notz & Worster, 2008; Worster & Rees Jones, 2015). Our method of estimating permeability is similar to that of Rees Jones and Worster (2014). We propose that if temperature fluctuations are observed at position z, then the harmonic mean bulk permeability over layer of thickness $(h-z)$ must marginally exceed a value that is appropriate for the critical value R_c. We can approximate the top of this layer as the position of the uppermost thermistor at which fluctuations occur and continue through to the thermistor immediately above the ice-ocean interface.

Table 2
List of Physical Parameters

Parameters		Value	Used in
Brine dynamic viscosity	μ	1.79×10^{-3} kg m^{-1} s^{-1}	Vancoppenolle et al. (2010)
Liquid density	ρ_ℓ	1,027 kg m^{-3}	Vancoppenolle et al. (2013)
Ice density	ρ_i	917 kg m^{-3}	Pringle et al. (2007)
Saline contraction coefficient	β	7.5×10^{-4} ppt^{-1}	Rees Jones and Worster (2014)
Sea ice thermal conductivity	k_{si}	$(\rho_{si}/\rho_i)[2.11-0.011T+0.09S_{si}/T-(\rho_{si}-\rho_i)/1000]$ W m^{-1} K^{-1}	Pringle et al. (2007)
Sea ice density	ρ_{si}	934 kg m^{-3}	Gough et al. (2012b)
Sea ice heat capacity	c_{si}	$[2.11+17.2S_{si}/(T^2)]\times10^3$ J kg^{-1} K	Untersteiner (1961)

The constants and parameters we select are listed in Table 2. For thermal diffusivity (κ_{si}) we use

$$\kappa_{si} = \frac{k_{si}}{\rho_{si} c_{si}}, \tag{6}$$

where k_{si}, ρ_{si}, and c_{si} are the sea ice thermal conductivity, density, and heat capacity, respectively (Table 2). Note that we use sea ice bulk salinity $S_{si} = 10$ ppt as a fixed value based on the upper bound of measurements by Gough et al. (2012a). This is also the upper bound of the salinity value that Pringle et al. (2007) used to optimize their k_{si} formulation.

Our permeability estimates need to be regarded with caution for the following reasons. First, the diffusion of a thermal anomaly from nearby cold brine channels toward the thermistor chain would cause a reduction in the magnitude of the temperature fluctuation. This results in an underestimation of the brine salinity difference between that level and that of the ocean underneath. Figure 1b helps visualize this. It can be seen in equation (4) that if the ΔS_b increases, permeability decreases. Second, we have assumed a constant value of critical Rayleigh number and have taken this value to be 10. It is uncertain and may vary by an order of magnitude. Third, our data are limited by the spacing of the thermistors which compromises our ability to identify the uppermost level at which convection takes place. Finally, thermal diffusivity plays a crucial role to the order of magnitude of permeability (Vancoppenolle et al., 2013). In our parameterization, κ_{si} (equation (6)) is in the range of $(0.4 \text{ to } 2.4)\times10^{-7}$m^2 s^{-1}.

2.4. Limitations

Temperature strings provide a one-dimensional measurement. As a result, we lack the information of the locations of the brine channels and tubes. To obtain the salinity of the brine, we must assume horizontal homogeneity and thermodynamic quasi-equilibrium locally between the brine channel and the sensor (see Lake & Lewis, 1970, for discussion). In reality, the temperature measured by the thermistor is the result of omnidirectional heat transfer from sources to the sensor. With fixed temperature string position, Niedrauer and Martin (1979) observed that temperature fluctuations can occur from lateral flow, and the closer the heat source, the higher the fluctuation. This will affect the estimation of brine salinity and whether the vertical or horizontal component of permeability dominates the measurement. Our sampling intervals of 4–10 min are similar to those of Lake and Lewis (1970) and Niedrauer and Martin (1979) (20 and 5 min intervals, respectively), so we are confident of detecting similar phenomena to these authors. The smallest temperature changes that the thermistor can resolve are listed as the resolution in Table 1.

3. Results

Large temperature fluctuations are generally confined to warm sea ice near the ice-ocean interface as expected. In sections 3.1 and 3.2, we consider statistically the influences of ice temperature and distance to the interface, respectively. Before analyzing these parameters, we describe typical features of the fluctuations as functions of time and depth, using the 2009B data set as an example (Figure 5).

There are two periods of larger temperature fluctuations (Figure 5b): from 20 July to 5 August, and from 9 September to the end of the record. The first matches the transition from columnar to incorporated platelet ice (Figure 5d) and might link to the first appearance of the sub-ice platelet layer in mid-July (Figure 5c).

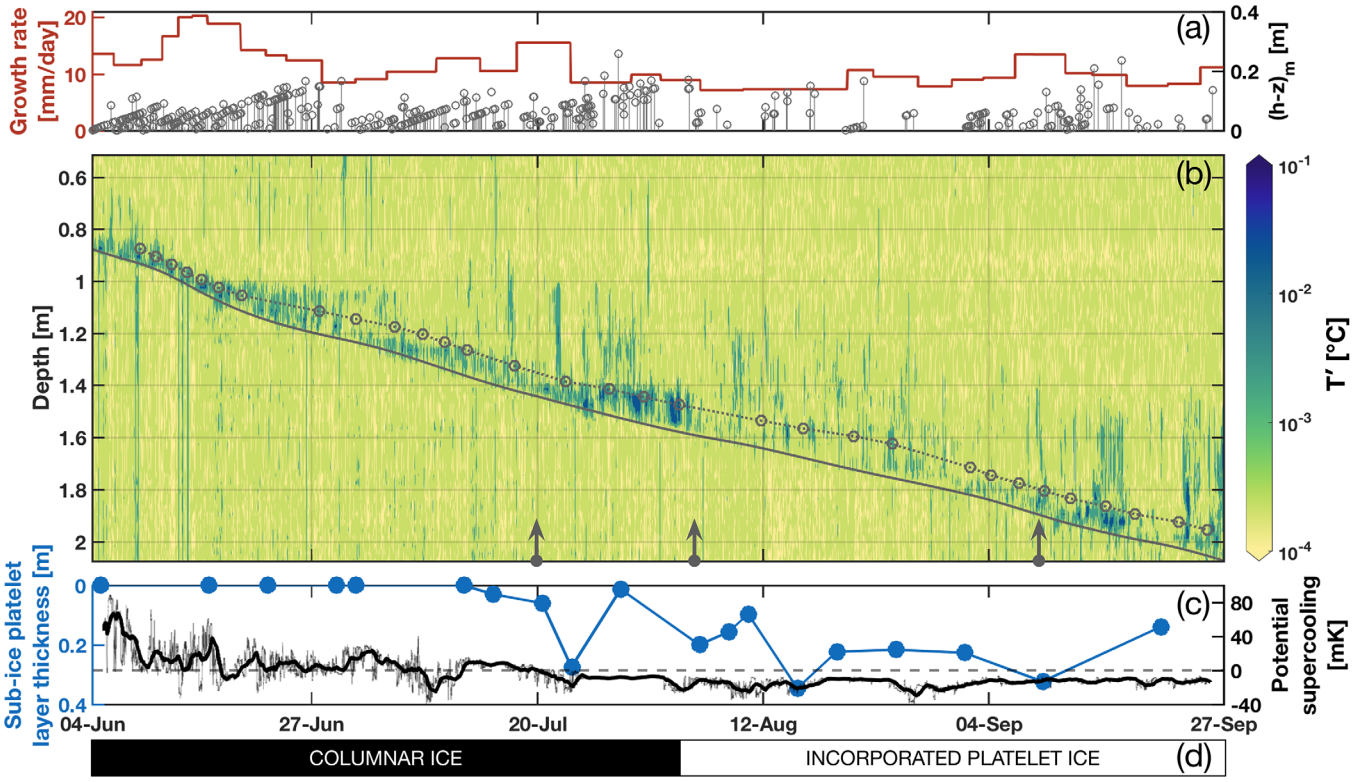

Figure 5. (a) Growth rate derived from thickness measurement and the estimated depth of convective region ($(h-z)_m$) discussed in section 3.4. (b) Magnitude of temperature fluctuations from 2009B, relative to the sea ice base (gray solid line) and −3°C (gray dotted line). The gray circles represent the times and locations of thermistors that reach a temperature of −3°C. The arrows mark dates of 20 July, 5 August, and 9 September 2009. (c) Observed sub-ice platelet layer thickness and potential supercooling measured at 50 m below the ocean surface at 2009B site (Gough et al., 2012b). (d) Timeline of whether columnar ice or incorporated platelet ice grew at the ice-water interface (Gough et al., 2012b).

This also coincided with the reduction in the growth rate (Figure 5a) which is a condition for the formation of a sub-ice platelet layer (Dempsey et al., 2010). The second, from early September, happened after the end of the polar night and when the top half of the ice was getting warmer (Figure 3b). This warming event potentially supported deep convection induced by warming the upper levels of the sea ice, as simulated by Griewank and Notz (2013). They induced deep convection in an idealized experiment by increasing the top temperature from −16.7°C to −5°C. In our data, the temperature at the top warmed from −25°C to −20°C during September and toward −10°C in November (Figure 3b). Note that $(h-z)_m$ in Figure 5a is determined as the position of the uppermost thermistor at which fluctuations occur and continue through to the thermistor immediately above the ice-ocean interface. This convective layer at the interface does not necessarily appear to be greatest at these times of deep convection.

3.1. Temperature Fluctuations Against Average Temperature

In this section, we consider the distribution of temperature fluctuations (T') with respect to their corresponding smoothed value T_{LOESS}. We select temperature bins of width ±0.05°C and centered on T_{LOESS}, i.e., T −0.05°C $< T_{LOESS} < T$ + 0.05°C. Within any 0.1°C window, there are of the order of 10^2–10^3 values of T', i.e., sufficiently large to allow for reliable statistical analyses. The interquartile range (IQR) and interdecile range (IDR; the range of data excluding the smallest 10% and largest 10%) of T' are then calculated for values of T_{LOESS} from −10°C to −1.85°C.

Results across the four data sets (2009A, 2009B, 2010, and 2013) are consistent. At temperatures of −10°C to −3°C, the level of variation in T' as determined by both the IQR and IDR is approximately constant (Figures 6a and 6b). As sea ice is generally impermeable when colder than −5°C (Golden et al., 1998; Weeks, 2010), these constant values provide estimates of the lowest practical values one could expect for T', i.e., what one might term a background noise level in the signal. Only above temperatures of approximately

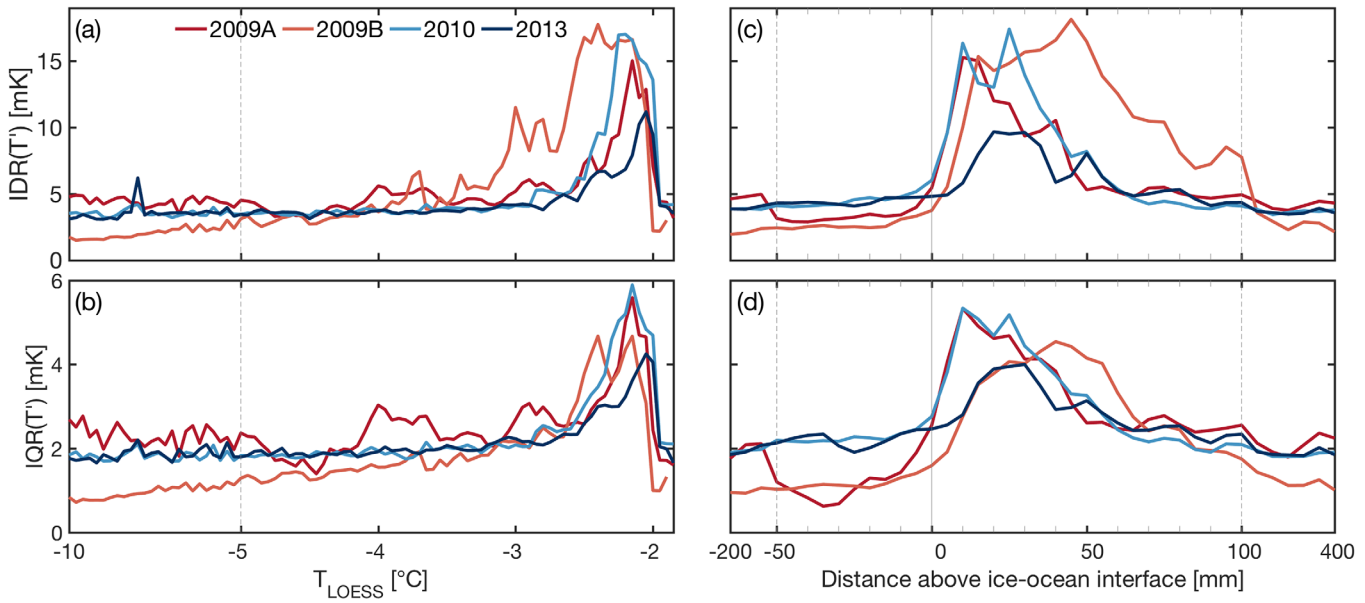

Figure 6. (a) The interdecile range and (b) the interquartile range of T' as a function of average sea ice temperature (T_{LOESS}). Note the fourfold change in scale on the horizontal axis either side of −5°C. (c) The interdecile range and (d) the interquartile range of T' as a function of proximity to the ice-ocean interface (negative values in the ocean). Note the 10-fold change in scale of the *x* axis below −50 mm and above 100 mm.

−3°C do we observe an increase in the variability of the signal for all data sets (Figures 6a and 6b). Large values of T' are not observed in the water because there is no significant temperature gradient there. There is a rapid decrease in temperature variation when the sea ice is slightly cooler than the freezing point (see Figures 6a and 6b). This occurs because the ±0.05°C window begins to include data recorded from thermistors in the ocean. Temperature fluctuations in this region are of similar magnitude to those in sea ice colder than −3°C.

3.2. Temperature Fluctuations Against Vertical Position

At the base of sea ice, there is a very porous layer with a thickness of the order of a few tens of millimeters (Backstrom & Eicken, 2006; Niedrauer & Martin, 1979; Petrich & Eicken, 2010; Weeks, 2010) over which the porosity approaches 100% with increasing depth. We can make an in situ estimate of the thickness of this layer using a similar analysis to the previous section: for any distance from the ice-ocean interface d_i, we include any data recorded by a thermistor within ±5 mm of d_i. To determine d_i for any thermistor we use estimated values of ice thickness as a function of time.

The variation in T' with distance above the ice-ocean interface is shown in Figures 6c and 6d. All data sets show that the maximum values of T' are <50 mm above the sea ice base, and there is an optimal distance where brine flow remains significant. Averaging the peaks in Figures 6c and 6d suggests this optimal distance is 20–25 mm above the ice-ocean interface. Values of IQR(T') and IDR(T') remain high over the next few tens of millimeters, typically dropping back down to their far-field values at a distance of 50–100 mm above the interface.

3.3. On-Percentage

Temperature fluctuations can be broadly categorized into two regimes based on whether the sea ice is warmer or cooler than approximately −3°C (see Figures 6a and 6b). We use this section to further investigate the temperature fluctuations for each thermistor after freezing by monitoring the temperature signal in two ranges: the freezing point to −3°C, and −3°C to −5°C. Figures 7a and 7b show fluctuations from the 2010 temperature sensor located at 1.5 m between the sensor's freezing time until T_{LOESS} reaches −3°C, and during −3°C to −5°C. Fluctuations started when the ice front reached and engulfed the thermistor on 17 July and ceased on 22 July when T_{LOESS} was slightly above −3°C similar to the result from section 3.1. It is apparent from Figure 7 that fluctuations in this example are confined within ±0.005°C in temperature range −3°C to −5°C.

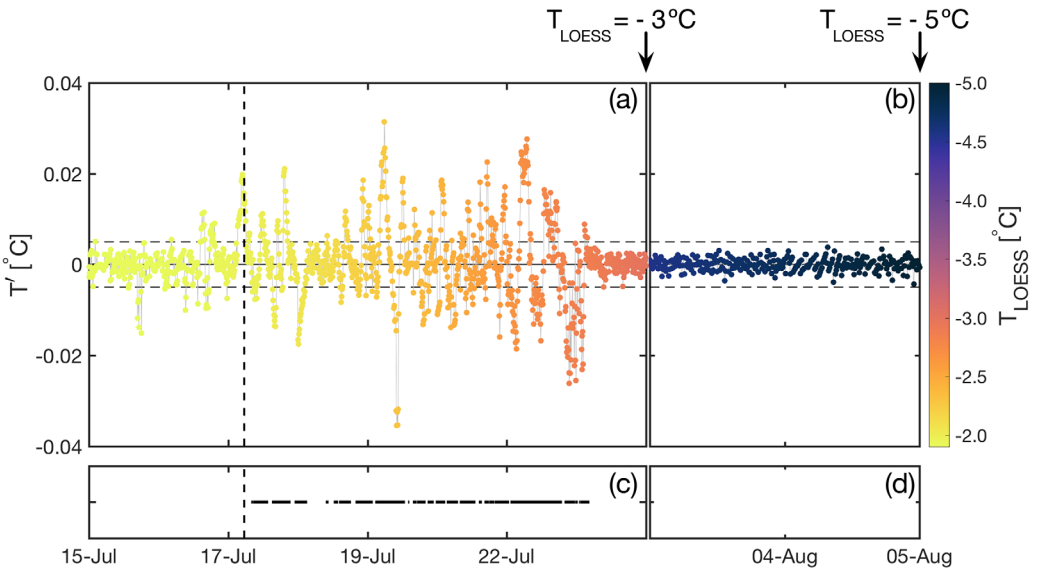

Figure 7. (a) Time series of temperature fluctuations (T') colored with the corresponding mean temperature (T_{LOESS}). Data for 2010 temperature string for the thermistor located at 1.50 m from the upper ice interface from the time when the ice-ocean interface reached the thermistor until a smoothed temperature of $T_{LOESS} = -3°C$. The vertical-dashed line marked the time when the ice front engulfed the thermistor. (b) Time period when $T_{LOESS} = -3°C$ to $-5°C$. Corresponding zero-crossing periods of Figures 7a and 7b, when the temperature signal passed the threshold ($\pm 0.005°C$), are marked with black horizontal lines in Figures 7c and 7d with the on-percentage 68% and 0%, respectively. Note the discontinuity of x axis after $T_{LOESS} = -3°C$ in Figures 7b and 7d.

We define brine convection as "on" when the absolute value of T' exceeds 0.005°C. The times between zero crossings are summed to yield a similar parameter to Middleton et al. (2016) which we call the on-percentage. It is calculated from temperature fluctuations not from direct observations of brine motion. In our context, on-percentage is calculated as the sum of all peak and trough widths (total length of horizontal black lines in Figures 7c and 7d) divided by the time interval for each region. For example, in Figure 7, the on-percentage in $T_{LOESS} > -3°C$ and $-3°C$ to $-5°C$ are 68% and 0%, respectively. Note also that we use only the data before the last thermistor froze in because we do not know the position of the interface after that. The results are plotted as a function of distance from the ice-ocean interface in Figure 8.

For thick sea ice, on-percentage is higher during temperatures $> -3°C$ than that during $-3°C$ to $-5°C$. Figure 8 is revealing in several ways. First, the on-percentage only exceeds 50% within 0.1 m of the interface and at temperatures greater than $-3°C$. Second, for ice temperatures between $-3°C$ and $-5°C$, the on-percentage is always less than 50%. Last, the on-percentage is larger close to the interface when the temperature of the sea ice is between the freezing point to $-3°C$ (43%) compared to $-3°C$ to $-5°C$ (11%).

3.4. Permeability From Temperature Fluctuations

Hypothetical Rayleigh number and vertical brine velocity profiles close to the ice-water interface are shown schematically in Figure 9. The value of R_c determines the true depth of the convective region, $(h-z)_c$. In our case, this depth is estimated as the position, $(h-z)_m$, of the uppermost thermistor that experiences temperature fluctuations at the same time as all thermistors embedded in the sea ice below also detect fluctuations. However, we cannot measure the vertical brine velocity profile because of the time resolution ($\approx$10 min) of our temperature measurements. The distribution of all $(h-z)_m$ estimates is shown in Figure 9c, where estimates are grouped according to whether they occur in columnar or incorporated platelet ice. The accuracy of these estimates of the depth of the convective region is limited to $\pm$half spacing of the thermistors (typically 30 or 50 mm). For example, assuming $T = -3°C$, if $(h-z)_c = 0.20 \pm 0.05$ m, Π varies from 5.9×10^{-11} to 9.8×10^{-11} m^2 when $\Delta S_b = 15$, and from 8.9×10^{-11} to 1.5×10^{-10} m^2 when $\Delta S_b = 10$. This affects the permeability estimation within about an order of magnitude depending on T (for κ_{si}) and ΔS_b (see Equation (4)). The means $\pm$ standard deviations of $(h-z)_m$ are 0.05 ± 0.04 and 0.04 ± 0.03 m for columnar and incorporated platelet ice, respectively.

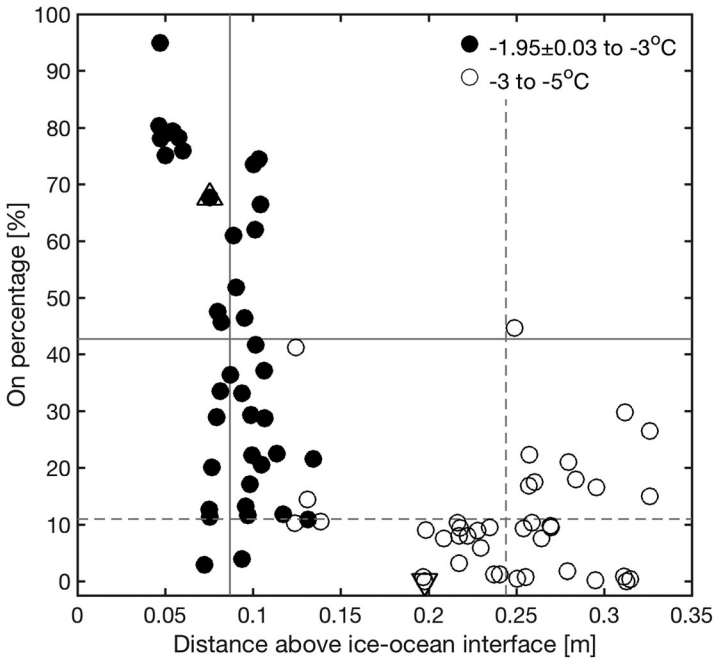

Figure 8. The on-percentage from the time a thermistor becomes frozen in -1.95 ± 0.03°C until the T_{LOESS} reached -3°C, and from -3°C to -5°C (see Figure 7, for an example) plotted against the distance between the ice-ocean interface and the thermistor when it reaches -3°C (solid circles) and -5°C (open circles). Note that data are excluded if they are from thermistors shallower than 0.5 m or if recorded less than 5 days after thermistor installation (see section 2.2). △ refers to Figure 7a and ▽ is Figure 7b. Horizontal solid lines and dashed lines mark 43% and 11% which are means of on-percentage for the -1.95 ± 0.03 to -3°C and -3°C to -5°C groups, respectively. Similarly, 0.09 and 0.24 m are the means of distance from ice-ocean interface when thermistors reached -3°C and -5°C, respectively.

Figure 10 shows harmonic mean permeabilities (Π) calculated using equation (4) with values of $(h-z)_m$ from Figure 9. Note that the harmonic mean permeability may alternatively be approximated as the permeability appropriate to the least permeable layer, as used by Notz and Worster (2008) and Vancoppenolle et al. (2010). Our data are again categorized into columnar and incorporated platelet ice, with arithmetic means of Π of approximately 3×10^{-9} m^2 for columnar and incorporated platelet ice. Our values are compared with measurements of vertical permeability using in situ bail tests during the Arctic spring/summer (Freitag & Eicken, 2003; Polashenski et al., 2017). The skewness and excess kurtosis (defined as kurtosis minus the kurtosis value for a normal distribution) for columnar and incorporated platelet ice are 6.3 and 47.8, and 6.8 and 55.4, respectively. Both skewness and excess kurtosis of permeability distributions of columnar and incorporated ice are greater than zero suggesting that their distributions are not normal. To explore the difference of the permeability distributions across the convective region of columnar and incorporated platelet ice, we apply a two-sample Kolmogorov-Smirnov test using kstest2 in the MATLAB Statistics and Machine Learning Toolbox version 10.2. Figure 10b shows the empirical cumulative distribution functions (ECDF) of the permeability histograms in Figure 10a as part of the Kolmogorov-Smirnov test.

4. Discussion

4.1. Characteristics of Temperature Fluctuations

Large temperature fluctuations are generally confined to ice warmer than about -3°C and within 75 mm of the ice-ocean interface throughout the four data sets analyzed here. This peak in the interdecile range of the temperature fluctuations (see Figures 6a and 6b) consistently lies between 10 and 17 mK on all three winters, indicating similar statistical dispersion in the temperature deviations from the mean. Thus in thick Antarctic sea ice our work directly confirms the view (Eide & Martin, 1975; Rees Jones & Worster, 2013) that convection is usually confined to a layer at the bottom of the sea ice.

However, there are variations in behavior of temperature fluctuations as winter progresses. Considering the particular example in Figure 5, we suggest that the denser and higher magnitude of temperature fluctuations in early August 2009 was due to the incorporated platelet ice transition (Figure 5d) which coincides with the first occurrence of a sub-ice platelet layer and with in situ supercooling in the near-surface ocean (Figure 5c) as reported in Leonard et al. (2006) and Gough et al. (2012b). The hiatus in late August is explained by the insulative effects of increased snow above, and sub-ice platelet layer below the sea ice. The higher magnitude fluctuations resume in early September 2009 and might be the signs of the arrival of polar summer (see Figure 3) which can also trigger convection (Fritsen et al., 1994; Griewank & Notz, 2013; Jardon et al., 2013; Widell et al., 2006).

All values of on-percentages greater than 50% belong within the 100 mm of the sea ice-water interface (Figure 8), reflecting the strong decrease in on-percentage with increasing distance from the ice-water interface. This result in Figure 8 matches those observed in earlier laboratory studies (Eide & Martin, 1975; Middleton et al., 2016) extending previous results into the natural environment of thick land-fast sea ice and long term observations. This has not been previously analyzed. An on-percentage of 10% or less for some thermistors might be explained by their positions relative to the brine drainage channels, as outlined in section 2.4.

The on-percentage analysis (Figure 8) confirms that the temperature fluctuations which are known to be discrete processes when studied visually in the laboratory (Eide & Martin, 1975; Middleton et al., 2016) and in Arctic columnar sea ice (Lake & Lewis, 1970), are also episodic in thick Antarctic land-fast sea ice. Indeed,

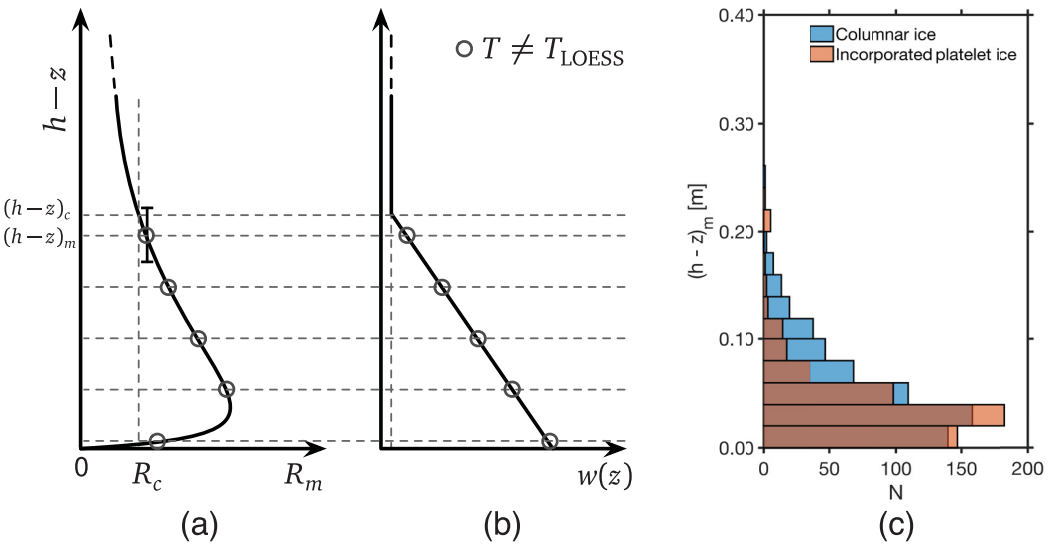

Figure 9. (a) Schematic of a typical Rayleigh number profile, where $h-z$ is the distance from the ice-ocean interface. Gray circles represent thermistors that show temperature fluctuations. $(h-z)_c$ is the true depth of the convective region constrained by critical Rayleigh number (R_c). $(h-z)_m$ is the measured estimate of $(h-z)_c$ taken as the uppermost depth at which fluctuations occur and continue through to the thermistor immediately above the ice-ocean interface. (b) Schematic of corresponding vertical profiles of vertical brine velocity (Rees Jones & Worster, 2014; Worster & Rees Jones, 2015). (c) Histogram of all $(h-z)_m$ measurements grouped into columnar (in blue) and incorporated platelet ice (in brown).

our finding of very few fluctuations in the -3°C to -5°C range suggest that in this range brine tubes shut down and disconnect into brine pockets (Light et al., 2003; Niedrauer & Martin, 1979). Occasionally events occur that extend 0.4–0.6 m upward from the ice-water interface and these may be examples of transient full-depth convection as predicted by Jardon et al. (2013), Rees Jones and Worster (2014), and Griewank and Notz (2013, 2015).

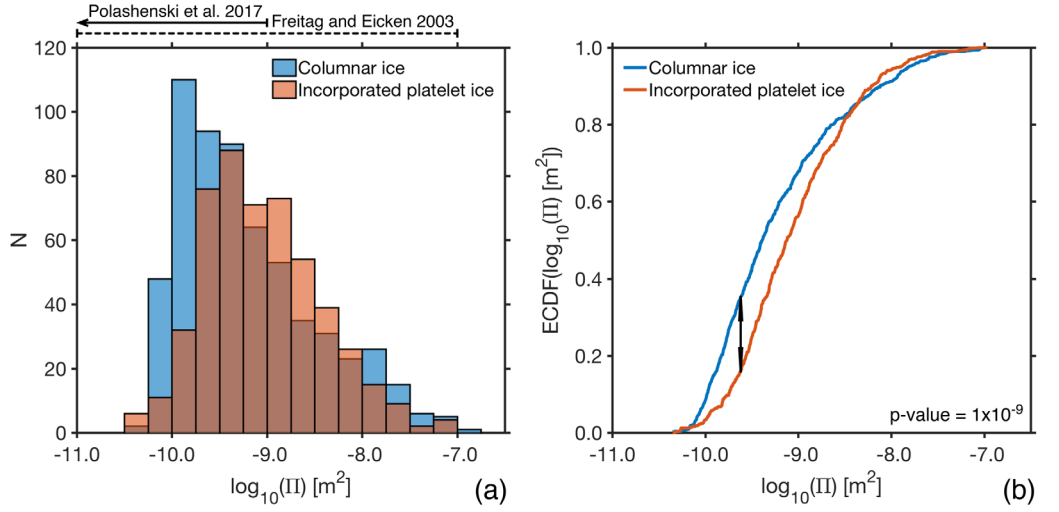

Figure 10. (a) Histogram of harmonic mean permeability (Π) from $(h-z)_m$ (Figure 9) to ice-ocean interface calculated from equation (4) categorized into columnar and incorporated platelet ice. Horizontal solid and dashed lines outline the range of vertical permeability in Arctic spring/summer sea ice (Freitag & Eicken, 2003; Polashenski et al., 2017). (b) Empirical cumulative distribution function (ECDF) plot of permeability in Figure 10a as part of the two-sample Kolmogorov-Smirnov test where the black line marks the maximum difference of ECDF between the two samples used to calculate the p-value.

4.2. Interpretation and Comparison of Permeability With Previous Studies

Our data provide evidence that the distribution of depths where convection takes place at the base of growing, winter Antarctic sea ice lies in the range 0–0.2 m with a mean of 0.05± 0.04 and 0.04± 0.03 m for columnar ice and incorporated platelet ice, respectively (Figure 9c). By comparing this value with other statistics of the distance above ice-ocean interface where temperature fluctuations take place of 0.05–0.1 m (section 3.2) and from the on-percentage of 0.09 to 0.24 m (section 3.3), a typical value of the thickness of convective layer can be estimated to be about 0.1 m. This range of values is in agreement with the critical thickness of the onset of convection in 13 laboratory experiments of approximately 0.02–0.08 m (Wettlaufer et al., 1997a), depending on initial solute concentration and the upper surface temperature. In particular, the mean is consistent with about 0.07 m when 3.55% by weight NaCl was used and surface temperature was set at −20°C (Wettlaufer et al., 1997b). The Antarctic mean also agrees with 0.02–0.03 m estimated from the young sea ice of approximately 0.2 m thickness in the Arctic (Notz & Worster, 2008).

Our estimates of harmonic mean permeability within 0.2 m of the ice-water interface lie between 10^{-10} and 10^{-7} m^2. This is in good agreement with the summer Arctic sea ice permeability measurements of Freitag and Eicken (2003), who report mean values of 4 and 8×10^{-10} m^2 for the lower sections of their ice cores on two separate cruises. Recent permeability measurements made on warm ($T > -2.7$°C), porous (>10%) Arctic sea ice lie in the range 10^{-13} and 10^{-9} m^2 (Polashenski et al., 2017), lower than the present estimates and those of Freitag and Eicken (2003).

In Figure 10, we compare the bulk permeabilities of two different sea ice structures: columnar and incorporated platelet ice. The null hypothesis of the Kolmogorov-Smirnov test is that the distributions of columnar and incorporated platelet ice permeability are drawn from the same population. From the two-sample Kolmogorov-Smirnov test, the p-value is 1×10^{-9} which is smaller than 0.01, implying the rejection of the null hypothesis at the 1% significance level. In conclusion, columnar and incorporated platelet ice have statistically significantly different permeability distributions but their arithmetic means are indistinguishable in the convective region.

5. Conclusion

Temperature fluctuations take place episodically and sporadically close to the sea ice-ocean interface and at warm temperatures. Most of the active period occurs when the temperature is above −3°C which is consistent with the findings from literature in laboratory-grown sea ice. Based on mushy layer theory, the bulk permeability of this layer at the base of thick (>1 m) land-fast Antarctic sea ice can be approximated from the temperature fluctuations and the results are within one order of magnitude of those obtained by other methods in the literature.

The cooling of sea ice from freezing point to −3°C takes place over an average of 0.09 m from the ice-ocean interface, and temperature fluctuations associated with brine movement in this layer are observed over 40% of the time. This on-percentage is reduced to about 10%, for ice that is greater than 0.15 m from the interface and is cooling from −3°C to −5°C.

Temperature fluctuations are extracted from in situ temperature data in thick Antarctic land-fast sea ice and used with a typical constant critical mushy-layer Rayleigh number of 10 (Worster, 1992). The same approach, but without mushy layer dynamics, was used by Lake and Lewis (1970) and Niedrauer and Martin (1979). We find that harmonic mean or bulk permeability has a magnitude of order 10^{-9} m^2 between 0 and 0.2 m from the ice-ocean interface. However the difference between the permeability distributions in the convective region of columnar and incorporated platelet ice is statistically significant. These permeabilities support the finding of Gough et al. (2012a) that the bulk salinity of columnar and incorporated platelet ice are only marginally different. This implies that we can apply the same parameterization of permeability to both columnar ice and incorporated platelet ice in thermodynamic sea ice models.

Acknowledgments

We gratefully acknowledge the logistical support of Antarctica New Zealand, Tim Haskell of Callaghan Innovation Ltd. and the winter-over crews of 2009, 2010, and 2013, who deployed temperature strings. We particularly thank Dr. Greg Leonard, Dr. Alex Gough, and Dr. Andy Mahoney for access to temperature and supporting data. Jono Everts assisted with calibration of 2010 and 2013 temperature data, and we are grateful to Grae Worster for useful discussions regarding mushy layer physics. P.W. was supported by a University of Otago Postgraduate Scholarship, and I.J.S.'s continued involvement in this project was supported by a number of University of Otago Research Grants. The study was also financially supported by New Zealand Foundation for Research Science and Technology contract IPY UOOX0705, and by subcontracts to National Institute of Water and Atmospheric Research (NIWA): project C01X1226 funded by Ministry of Business, Innovation and Employment; and numerous core funding projects, most recently CAOA1703. We acknowledge two anonymous reviewers and the editors, whose suggestions and comments helped improve the earlier version of the manuscript. The temperature data used in this study from 2009A, 2009B, 2010, and 2013 can be obtained from https://doi.pangaea.de/10.1594/PANGAEA.880162, https://doi.pangaea.de/10.1594/PANGAEA.880163, https://doi.pangaea.de/10.1594/PANGAEA.880164, and https://doi.pangaea.de/10.1594/PANGAEA.880165, respectively.

References

Arrigo, K. R., Mock, T., & Lizotte, M. P. (2010). Primary producers and sea ice. In D. N. Thomas & G. S. Dieckmann (Eds.), *Sea ice* (2nd ed., pp. 283–325). Oxford, UK: Wiley-Blackwell. https://doi.org/10.1002/9781444317145.ch8

Backstrom, L. G., & Eicken, H. (2006). Capacitance probe measurements of brine volume and bulk salinity in first-year sea ice. *Cold Regions Science and Technology*, *46*(3), 167–180. https://doi.org/10.1016/j.coldregions.2006.08.018

Cleveland, W. S. (1979). Robust locally weighted regression and smoothing scatterplots. *Journal of the American Statistical Association*, *74*(368), 829–836. https://doi.org/10.1080/01621459.1979.10481038

Cox, G. F. N., & Weeks, W. F. (1975). Brine drainage and initial salt entrapment in sodium chloride ice (*Tech. Rep. CRREL Res. Rep. 345*), Hanover, NH: U.S. Army Cold Regions Research and Engineering Laboratory.

Dempsey, D. E., Langhorne, P. J., Robinson, N. J., Williams, M. J. M., Haskell, T. G., & Frew, R. D. (2010). Observation and modeling of platelet ice fabric in McMurdo Sound, Antarctica. *Journal of Geophysical Research*, *115*, C01007. https://doi.org/10.1029/2008JC005264

Eicken, H., Grenfell, T. C., Perovich, D. K., Richter-Menge, J. A., & Frey, K. (2004). Hydraulic controls of summer Arctic pack ice albedo. *Journal of Geophysical Research*, *109*, C08007. https://doi.org/10.1029/2003JC001989

Eide, L. I., & Martin, S. (1975). The formation of brine drainage features in young sea ice. *Journal of Glaciology*, *14*(70), 137–154. https://doi.org/10.1017/s0022143000013460

Feltham, D. L., Untersteiner, N., Wettlaufer, J. S., & Worster, M. G. (2006). Sea ice is a mushy layer. *Geophysical Research Letters*, *33*, L14501. https://doi.org/10.1029/2006GL026290

Freitag, J. (1999). The hydraulic properties of Arctic sea-ice—Implications for the small scale particle transport. *Reports on Polar Research*, *325*, 1–150.

Freitag, J., & Eicken, H. (2003). Meltwater circulation and permeability of Arctic summer sea ice derived from hydrological field experiments. *Journal of Glaciology*, *49*(166), 349–358. https://doi.org/10.3189/172756503781830601

Fritsen, C. H., Lytle, V. I., Ackley, S. F., & Sullivan, C. W. (1994). Autumn bloom of Antarctic pack-ice algae. *Science*, *266*(5186), 782–784. https://doi.org/10.1126/science.266.5186.782

Golden, K. M., Ackley, S. F., & Lytle, V. I. (1998). The percolation phase transition in sea ice. *Science*, *282*(5397), 2238–2241. https://doi.org/10.1126/science.282.5397.2238

Gough, A. J., Mahoney, A. R., Langhorne, P. J., Williams, M. J. M., & Haskell, T. G. (2012a). Sea ice salinity and structure: A winter time series of salinity and its distribution. *Journal of Geophysical Research*, *117*, C03008. https://doi.org/10.1029/2011JC007527

Gough, A. J., Mahoney, A. R., Langhorne, P. J., Williams, M. J., Robinson, N. J., & Haskell, T. G. (2012b). Signatures of supercooling: McMurdo Sound platelet ice. *Journal of Glaciology*, *58*(207), 38–50. https://doi.org/10.3189/2012JoG10J218

Griewank, P. J., & Notz, D. (2013). Insights into brine dynamics and sea ice desalination from a 1-D model study of gravity drainage. *Journal of Geophysical Research: Oceans*, *118*, 3370–3386. https://doi.org/10.1002/jgrc.20247

Griewank, P. J., & Notz, D. (2015). A 1-d modelling study of Arctic sea-ice salinity. *The Cryosphere*, *9*(1), 305–329. https://doi.org/10.5194/tc-9-305-2015

Jardon, F. P., Vivier, F., Vancoppenolle, M., Lourenço, A., Bouruet-Aubertot, P., & Cuypers, Y. (2013). Full-depth desalination of warm sea ice. *Journal of Geophysical Research: Oceans*, *118*, 435–447. https://doi.org/10.1029/2012JC007962

Lake, R. A., & Lewis, E. L. (1970). Salt rejection by sea ice during growth. *Journal of Geophysical Research*, *75*(3), 583–597. https://doi.org/10.1029/JC075i003p00583

Langhorne, P. J., Hughes, K. G., Gough, A. J., Smith, I. J., Williams, M. J. M., Robinson, N. J.,. . . Haskell, T. G. (2015). Observed platelet ice distributions in Antarctic sea ice: An index for ocean-ice shelf heat flux. *Geophysical Research Letters*, *42*, 5442–5451. https://doi.org/10.1002/2015GL064508

Leonard, G. H., Langhorne, P. J., Williams, M. J. M., Vennell, R., Purdie, C. R., Dempsey, D. E.,. . . Frew, R. D. (2011). Evolution of supercooling under coastal Antarctic sea ice during winter. *Antarctic Science*, *23*(4), 399–409. https://doi.org/10.1017/S0954102011000265

Leonard, G. H., Purdie, C. R., Langhorne, P. J., Haskell, T. G., Williams, M. J. M., & Frew, R. D. (2006). Observations of platelet ice growth and oceanographic conditions during the winter of 2003 in McMurdo Sound, Antarctica. *Journal of Geophysical Research*, *111*, C04012. https://doi.org/10.1029/2005JC002952

Lewis, E. L. (1967). Heat flow through winter ice. In H. Oura (Ed.), *Physics of ice and snow, international conference on low temperature science, proceedings* (Vol. 1(1), pp. 611–631). Sapporo, Japan: Hokkaido University.

Light, B., Maykut, G. A., & Grenfell, T. C. (2003). Effects of temperature on the microstructure of first-year Arctic sea ice. *Journal of Geophysical Research*, *108*(C2), 3051. https://doi.org/10.1029/2001JC000887

Maksym, T., & Jeffries, M. O. (2000). A one-dimensional percolation model of flooding and snow ice formation on Antarctic sea ice. *Journal of Geophysical Research*, *105*(C11), 26313–26331. https://doi.org/10.1029/2000JC900130

Middleton, C. A., Thomas, C., De Wit, A., & Tison, J. L. (2016). Visualizing brine channel development and convective processes during artificial sea-ice growth using Schlieren optical methods. *Journal of Glaciology*, *62*(231), 1–17. https://doi.org/10.1017/jog.2015.1

Niedrauer, T. M., & Martin, S. (1979). An experimental study of brine drainage and convection in young sea ice. *Journal of Geophysical Research*, *84*(C3), 1176. https://doi.org/10.1029/JC084ic03p01176

Notz, D. (2005). *Thermodynamic and fluid-dynamical processes in sea ice* (PhD thesis). Cambridge, UK: University of Cambridge.

Notz, D., & Worster, M. G. (2008). In situ measurements of the evolution of young sea ice. *Journal of Geophysical Research*, *113*, C03001. https://doi.org/10.1029/2007JC004333

Notz, D., & Worster, M. G. (2009). Desalination processes of sea ice revisited. *Journal of Geophysical Research*, *114*, C05006. https://doi.org/10.1029/2008JC004885

Petrich, C., & Eicken, H. (2010). Growth, structure and properties of sea ice. In D. N. Thomas & G. S. Dieckmann (Eds.), *Sea ice* (2nd ed., pp. 23–77). Oxford, UK: Wiley-Blackwell. https://doi.org/10.1002/9781444317145.ch2

Petrich, C., Langhorne, P. J., & Sun, Z. F. (2006). Modelling the interrelationships between permeability, effective porosity and total porosity in sea ice. *Cold Regions Science and Technology*, *44*(2), 131–144. https://doi.org/10.1016/j.coldregions.2005.10.001

Polashenski, C., Golden, K. M., Perovich, D. K., Skyllingstad, E., Arnsten, A., Stwertka, C., & Wright, N. (2017). Percolation blockage: A process that enables melt pond formation on first year Arctic sea ice. *Journal of Geophysical Research: Oceans*, *122*, 413–440. https://doi.org/10.1002/2016JC011994

Pringle, D. J., Eicken, H., Trodahl, H. J., & Backstrom, L. G. E. (2007). Thermal conductivity of landfast Antarctic and Arctic sea ice. *Journal of Geophysical Research*, *112*, C04017. https://doi.org/10.1029/2006JC003641

Reeburgh, W. S. (1984). Fluxes associated with brine motion in growing sea ice. *Polar Biology*, *3*(1), 29–33. https://doi.org/10.1007/BF00265564

Rees Jones, D. W., & Worster, M. G. (2013). A simple dynamical model for gravity drainage of brine from growing sea ice. *Geophysical Research Letters*, *40*, 307–311. https://doi.org/10.1029/2012GL054301

Rees Jones, D. W., & Worster, M. G. (2014). A physically based parameterization of gravity drainage for sea-ice modeling. *Journal of Geophysical Research: Oceans*, *119*, 5599–5621. https://doi.org/10.1002/2013JC009296

Smith, I. J., Langhorne, P. J., Frew, R. D., Vennell, R., & Haskell, T. G. (2012). Sea ice growth rates near ice shelves. *Cold Regions Science and Technology*, *83–84*, 57–70. https://doi.org/10.1016/j.coldregions.2012.06.005

Tedesco, L., Vichi, M., Haapala, J., & Stipa, T. (2010). A dynamic biologically active layer for numerical studies of the sea ice ecosystem. *Ocean Modelling*, *35*(1–2), 89–104. https://doi.org/10.1016/j.ocemod.2010.06.008

Trodahl, H. J., McGuinness, M. J., Langhorne, P. J., Collins, K., Pantoja, A. E., Smith, I. J., & Haskell, T. G. (2000). Heat transport in McMurdo Sound first-year fast ice. *Journal of Geophysical Research*, *105*(C5), 11347–11358. https://doi.org/10.1029/1999JC000003

Turner, A. K., & Hunke, E. C. (2015). Impacts of a mushy-layer thermodynamic approach in global sea-ice simulations using the CICE sea-ice model. *Journal of Geophysical Research: Oceans*, *120*, 1253–1275. https://doi.org/10.1002/2014JC010358

Turner, A. K., Hunke, E. C., & Bitz, C. M. (2013). Two modes of sea-ice gravity drainage: A parameterization for large-scale modeling. *Journal of Geophysical Research: Oceans*, *118*, 2279–2294. https://doi.org/10.1002/jgrc.20171

Untersteiner, N. (1961). On the mass and heat budget of Arctic sea ice. *Archiv für Meteorologie, Geophysik und Bioklimatologie Serie A*, *12*(2), 151–182. https://doi.org/10.1007/bf02247491

Untersteiner, N. (1968). Natural desalination and equilibrium salinity profile of perennial sea ice. *Journal of Geophysical Research*, *73*(4), 1251–1257. https://doi.org/10.1029/JB073i004p01251

Vancoppenolle, M., Goosse, H., de Montety, A., Fichefet, T., Tremblay, B., & Tison, J.-L. (2010). Modeling brine and nutrient dynamics in Antarctic sea ice: The case of dissolved silica. *Journal of Geophysical Research*, *115*, C02005. https://doi.org/10.1029/2009JC005369

Vancoppenolle, M., Notz, D., Vivier, F., Tison, J., Delille, B., Carnat, G.,. . . Haskell, T. (2013). Technical note: On the use of the mushy-layer Rayleigh number for the interpretation of sea-ice-core data. *The Cryosphere Discussions*, *7*(4), 3209–3230. https://doi.org/10.5194/tcd-7-3209-2013

Weeks, W. (2010). *On sea ice*. University of Alaska Press.

Wells, A. J., Wettlaufer, J. S., & Orszag, S. A. (2010). Maximal potential energy transport: A variational principle for solidification problems. *Physical Review Letters*, *105*, 254–502. https://doi.org/10.1103/PhysRevLett.105.254502

Wells, A. J., Wettlaufer, J. S., & Orszag, S. A. (2011). Brine fluxes from growing sea ice. *Geophysical Research Letters*, *38*, L04501. https://doi.org/10.1029/2010GL046288

Wettlaufer, J. S., Grae Worster, M., & Huppert, H. E. (1997a). Natural convection during solidification of an alloy from above with application to the evolution of sea ice. *Journal of Fluid Mechanics*, *344*, 291–316. https://doi.org/10.1017/S0022112097006022

Wettlaufer, J. S., Worster, M. G., & Huppert, H. E. (1997b). The phase evolution of young sea ice. *Geophysical Research Letters*, *24*(10), 1251–1254. https://doi.org/10.1029/97GL00877

Widell, K., Fer, I., & Haugan, P. M. (2006). Salt release from warming sea ice. *Geophysical Research Letters*, *33*, L12501. https://doi.org/10.1029/2006GL026262

Worster, M. G. (1992). Instabilities of the liquid and mushy regions during solidification of alloys. *Journal of Fluid Mechanics*, *237*(1), 649. https://doi.org/10.1017/s0022112092003562

Worster, M. G., & Rees Jones, D. W. (2015). Sea-ice thermodynamics and brine drainage. *Philosophical Transactions of the Royal Society A: Mathematical, Physical and Engineering Sciences*, *373*(2045), 20140166. https://doi.org/10.1098/rsta.2014.0166